THEORETICAL AND APPLIED MECHANICS
Volume 46 (2019) Issue 2, 191–219 DOI: https://doi.org/10.2298/TAM190911012A

AXISYMMETRIC ELASTICITY SOLUTION FOR AN UNDRAINED SATURATED PORO-PIEZOELASTIC THICK DISK

Ali Abjadi, Mohsen Jabbari, and Ahmad Reza Khorshidvand

Abstract. In this paper, a circular thick plate made of poroelastic piezoelectric ceramic is studied. The porosities of the plate vary through the thickness and axisymmetric behavior of a piezoelectric disk exhibiting hexagonal material symmetry of class 6 mm. Additionally, external mechanical loads which are in axi-symmetric general form act on the plate. The material properties of the plate vary exponentially as functions of the z variable in cylindrical coordinates. Based on an elasticity solution in terms of radial and axial displacements (u, w), the governing partial differential equations are derived and solved analytically; mechanical stresses and electric displacements are then calculated. Finally an example which illustrates the application of the derived formulas is presented.

1. Introduction

Axisymmetric problems of piezoelectric materials are enormously popular with researchers. A. B. Dobrucki et al. presented a theory of axisymmetric piezoelectric bimorph which consists of two or more layers placed asymmetrically to the middle surface of the structures [1]. They solved the derived equations by finite element method. H. J. Ding et al. investigated the transient responses of axisymmetric plane strain problems for a piezoelectric hollow cylinder [2]. They transferred the partial differential equations to an integral equation about a function with respect to time and solved them successfully by means of interpolation method. W. Zi-Kung et al. presented a general solution and the application of space axisymmetric piezoelectric using the method of introducing potential functions one by one [3]. S. Kapuria et al. put forth a 3D-solution for a simply supported piezoelectric cylindrical shell subjected to axisymmetric electromechanical load. They employed Fourier and power series and an exponential function to solve governing

2010 *Mathematics Subject Classification:* 33C10; 35J57; 35Q47; 35Q79.
Key words and phrases: circular plate, porous material, mechanical stresses, piezoelectric, elasticity solution.

differential equations [4]. N. Kharouf and P. R. Heyliger studied a numerical approximate solution to static and axisymmetric vibration problems for piezoelectric cylinders, including those composed of more than one material [5]. F. Ebrahimi et al. presented an analytical solution for axisymmetric free vibrations of an FG thick circular plate integrated with piezoelectric (PZT4) layers based on Mindlin plate theory [6]. They solved the differential equations analytically for clamped and simply-supported edge. F. Ashida et al. examined the transient solution for a piezothermoelastic circular disk under axisymmetric heating. They used a potential function to find the exact solution for equilibrium and electrostatic equations [7]. S. Kapuria et al. found the exact solution for an axisymmetric piezothermoelastic simply-supported hybrid cylindrical shell made of cross-ply composite laminate and piezoelectric layers [8]. J. Sladek et al. used the meshless local Petrov–Galerkin (MLPG) method to investigate the 3D-dynamic response of axisymmetric piezoelectric solids with continuously nonhomogeneous material properties. They consider a 3D axisymmetric body created by revolution of cross section around an axis of symmetry with mechanical and thermal loads [9]. S. Dong et al. studied an analytical solution to calculate the transverse deflection shape of circular axisymmetric piezoelectric metal composite unimorph actuators. Their solutions account for both the influence of an applied electric field and a concentrated or uniformly distributed mechanical load [10]. W. X. Zhang et al. present an exact solution for the deformation and stress field in a finite cylinder under axisymmetric boundary conditions. They formulated the problem based on the state space formulation for a transversely isotropic piezoelectric material [11]. P. Zhang et al. introduced precise integration algorithm (PIA) to formulate an axisymmetric multi-layered transversely isotropic piezoelectric body [12]. S. S. Volkvo et al. studied an FG piezoelectric electroelastic half-space [13]. They consider elastic moduli and dielectric permeabilities of the coating, which vary independently with depth according to arbitrary functions. M. Ishihara et al. analyzed the thermoelectro elastic solid cylinder with D_∞ symmetry under axisymmetric mechanical and thermal loading [14]. They consider distributed torsional shear stress as a mechanical load and nonuniform temperature distribution as a thermal disturbance. J. Liu et al. found a solution for a multilayered transversely isotropic piezoelectric system based on the precise integration algorithm (PIA) and the technique of dual vector under axisymmetric load [15]. T. J. Liu et al. studied an axisymmetric indentation problem of a perfect rigid electrical insulator indenter on an FG piezoelectric coating bonded to a piezoelectric substrate. They consider material properties to be exponentially varied along the thickness [16]. X. Zhao et al. put forth an axisymmetric analytical solution for a heterogeneous transversely isotropic multi-ferroic circular plate subjected to electric loading. They considered the coupling magneto-electro-elastic fields which exactly satisfy the upper and lower boundary conditions and approximately meet the cylindrical boundary condition [17]. Porous piezoelectric ceramics have many applications in industry such as nondestructive tests, medical ultrasonic devices, low frequency hydrophones, contact microphones, underwater acoustics, vibratory sensors, and so forth [18–22]. M. L. Dunn and M. Taya forwarded a theoretical approach to predict the electromechanical properties of porous piezoelectric ceramics.

They accounted for the effects of porosity shape and concentration [23]. E. Roncari et al. examined the piezoelectric porous lead zirconate titanate ceramics. They studied the effect of polymer volume and sintering temperature on microstructure samples [24].

In this paper, a circular thick disk made of poroelastic piezoelectric material (hexagonal material symmetry of class 6 mm) is considered. General mechanical and electrical loads act at lower and upper surfaces of the disk. The plate is considered undrained and saturated from a poroelastic point of view. The porosities of disk vary through the thickness; thus, material properties are considered as exponential functions of the axial variable "z" in cylindrical coordinates. The method of derivation of the governing equation is based on elasticity approach in terms of displacements and electrical potential function. These equations are solved directly without using Love stress functions, which facilitates handling any general boundary conditions.

2. Mathematics

The axisymmetric behavior of a porous piezoelectric circular thick disk exhibiting hexagonal material symmetry of class 6 mm is illustrated schematically in Figure 1.

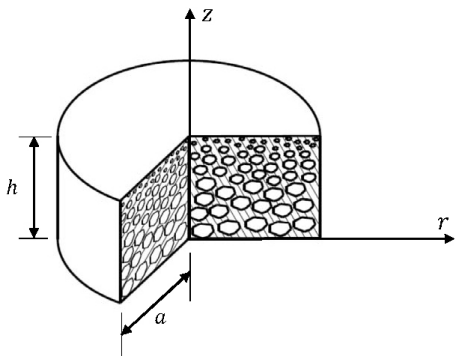

FIGURE 1. Schematic of a poroelastic circular thick disk

The constitutive relations for the elastic field, expressed in cylindrical coordinates, for a circular plate are

$$\begin{aligned}
\sigma_{rr} &= c_{11}\varepsilon_{rr} + c_{12}\varepsilon_{\theta\theta} + c_{13}\varepsilon_{zz} - e_{31}E_z - \gamma p \\
\sigma_{\theta\theta} &= c_{12}\varepsilon_{rr} + c_{22}\varepsilon_{\theta\theta} + c_{23}\varepsilon_{zz} - e_{32}E_z - \gamma p \\
\sigma_{zz} &= c_{13}\varepsilon_{rr} + c_{23}\varepsilon_{\theta\theta} + c_{33}\varepsilon_{zz} - e_{33}E_z - \gamma p \\
\sigma_{rz} &= 2c_{55}\varepsilon_{rz} - e_{15}E_r \\
E_r &= -\frac{\partial\phi}{\partial r} \qquad E_z = -\frac{\partial\phi}{\partial z}
\end{aligned} \tag{2.1}$$

where σ_{ij}, $\varepsilon_{ij}(i,j = r,\theta,z)$, C_{ij}, e_{ij}, E_i, γ, p, ϕ are the stress tensor, strain tensor, elastic stiffnesses, Piezoelectric coefficients, electric field intensities, Biot's

coefficient of effective stress, pressure in the porous media, and electric potential, respectively. Here p is related to Biot's modulus, volumetric strain, and the variation of fluid content. The under undrained condition as

$$P = -M\gamma(\varepsilon_{rr} + \varepsilon_{\theta\theta} + \varepsilon_{zz}) \tag{2.2}$$

and

$$M = \frac{2\mu(v_u - v)}{\gamma^2(1-2v)(1-2v_u)} \qquad \mu = \frac{E_0}{2(1+v)} \tag{2.3}$$

where M, μ, ν, ν_u, E_0 are Biot's modulus, shear modulus, poisson's ratio, undrained poisson's ratio, and material constant, respectively. And

$$\begin{aligned} &c_{11} + M\gamma^2 = c_{11}^* \quad c_{12} + M\gamma^2 \quad = c_{12}^* \quad c_{13} + M\gamma^2 = c_{13}^* \\ &c_{22} + M\gamma^2 = c_{22}^* \quad c_{23} + M\gamma^2 \quad = c_{23}^* \quad c_{33} + M\gamma^2 = c_{33}^* \quad c_{55} \quad = c_{55}^* \end{aligned} \tag{2.4}$$

Thus

$$\begin{aligned} \sigma_{rr} &= c_{11}^*\varepsilon_{rr} + c_{12}^*\varepsilon_{\theta\theta} + c_{13}^*\varepsilon_{zz} - e_{31}E_z \\ \sigma_{\theta\theta} &= c_{12}^*\varepsilon_{rr} + c_{22}^*\varepsilon_{\theta\theta} + c_{23}^*\varepsilon_{zz} - e_{32}E_z \\ \sigma_{zz} &= c_{13}^*\varepsilon_{rr} + c_{23}^*\varepsilon_{\theta\theta} + c_{33}^*\varepsilon_{zz} - e_{33}E_z \\ \sigma_{rz} &= 2c_{55}^*\varepsilon_{rz} - e_{15}E_r \end{aligned} \tag{2.5}$$

The strains are related to the displacements u and w by

$$\varepsilon_{rr} = u_{,r} \quad \varepsilon_{\theta\theta} = \tfrac{1}{r}u \quad \varepsilon_{zz} = w_{,z} \quad \varepsilon_{rz} = \tfrac{1}{2}(w_{,r} + u_{,z}) \quad \varepsilon_{r\theta} = \varepsilon_{\theta z} = 0 \tag{2.6}$$

where $(\,,)$ denotes the partial derivative. The constitutive equations for the electric field are

$$D_{rr} = 2e_{15}\varepsilon_{rz} + \eta_{11}E_r \qquad D_{zz} = e_{31}\varepsilon_{rr} + e_{32}\varepsilon_{\theta\theta} + e_{33}\varepsilon_{zz} + \eta_{33}E_z \tag{2.7}$$

where D_{ii} are electric displacement components and η_{ii} are dielectric permittivities. The equilibrium equations in radial and axial directions, disregarding the body forces, are

$$\begin{aligned} &\frac{\partial\sigma_{rr}}{\partial r} + \frac{\partial\sigma_{rz}}{\partial z} + \frac{1}{r}(\sigma_{rr} - \sigma_{\theta\theta}) = 0 \qquad \frac{\partial\sigma_{rz}}{\partial r} + \frac{\partial\sigma_{zz}}{\partial z} + \frac{1}{r}\sigma_{rz} = 0 \\ &\frac{\partial D_{rr}}{\partial r} + \frac{\partial D_{zz}}{\partial z} + \frac{1}{r}(D_{rr}) = 0. \end{aligned} \tag{2.8}$$

To obtain the equilibrium equations in terms of the displacement components for the porous piezoelectric circular plate, the functional relationship of the material properties must be known. Therefore, the plate material is assumed to be porous across the z-direction and the modulus is elasticity are assumed to be described by the exponential functions as

$$C_{ij}^* = \overline{C^*}_{ij}e^{m(\frac{z}{h})} \qquad e_{ij} = \bar{e}_{ij}e^{m(\frac{z}{h})} \qquad \eta_{ij} = \bar{\eta}_{ij}e^{m(\frac{z}{h})} \tag{2.9}$$

In the relations (2.9), $\overline{C^*}_{ij}$, $\bar{e}_{ij}$, $\bar{\eta}_{ij}$ are the material constants at a lower surface in $z = 0$. For the isotropic and hexagonal symmetry of class 6 mm, the following relations are considered as

$$C_{11}^* = C_{22}^* = C_{33}^* \qquad C_{12}^* = C_{21}^* = C_{13}^* = C_{31}^* = C_{23}^* = C_{32}^* \qquad e_{31} = e_{32} \tag{2.10}$$

Using the relations (2.1)–(2.10), the Navier equations in terms of the displacement components are

$$u_{,rr}+\frac{1}{r}u_{,r}-\frac{1}{r^2}u+d_1u_{,z}+d_2u_{,zz}+d_3w_{,rz}+d_1w_{,r}+d_4\phi_{,rz}+d_5\phi_{,r}=0 \tag{2.11}$$

$$w_{,rr}+\frac{1}{r}w_{,r}+d_6w_{,z}+d_7w_{,zz}+d_8\Big(u_{,rz}+\frac{1}{r}u_{,z}\Big)+d_9\Big(u_{,r}+\frac{1}{r}u\Big)+d_{10}\Big(\phi_{,rr}+\frac{1}{r}\phi_{,r}\Big)+d_{11}\phi_{,z}+d_{12}\phi_{,zz}=0 \tag{2.12}$$

$$\phi_{,rr}+\frac{1}{r}\phi_{,r}+d_{13}\phi_{,zz}+d_{14}\phi_{,z}-d_{15}w_{,zz}-d_{16}w_{,z}-d_{17}\Big(w_{,rr}+\frac{1}{r}w_{,r}\Big)-d_{18}\Big(u_{,rz}+\frac{1}{r}u_{,z}\Big)+d_{19}\Big(u_{,r}+\frac{1}{r}u\Big)=0 \tag{2.13}$$

where constants d_1 to d_{19} are given in Appendix. Eqs. (2.11), (2.12) and (2.13) are a system of homogeneous partial differential equations with variable coefficients (functions of radial variable r).

3. Solution

Since the coefficients of Eqs. (2.11), (2.12) and (2.13) are independent of the variable z, the exponential function form of the coordinate z may be assumed for the general solution as

$$u(r,z)=U(r)e^{Pz} \tag{3.1a}$$

$$w(r,z)=W(r)e^{Pz}+F_1(z) \tag{3.1b}$$

$$\phi(r,z)=\Phi(r)e^{Pz}+F_2(z) \tag{3.1c}$$

Substituting (3.1) in the Navier Eqs. (2.11), (2.12), (2.13) gives

$$U''+\frac{1}{r}U'-\frac{1}{r^2}U+(d_2P^2+d_1P)U+(d_3P+d_1)W'+(d_4P+d_5)\Phi'=0 \tag{3.2}$$

$$[W''+\tfrac{1}{r}W'+(d_7P^2+d_6P)W+(d_8P+d_9)(U'+\tfrac{1}{r}U)+d_{10}(\Phi''+\tfrac{1}{r}\Phi')+(d_{12}P^2+d_{11}P)\Phi]+[d_7F_1''(z)+d_6F_1'(z)+d_{12}F_2''(z)+d_{11}F_2'(z)]e^{-Pz}=0 \tag{3.3}$$

$$[\Phi''+\tfrac{1}{r}\Phi'+(d_{13}P^2+d_{14}P)\Phi-(d_{15}P^2+d_{16}P)W-d_{17}(W''+\tfrac{1}{r}W')-(d_{18}P+d_{19})(U'+\tfrac{1}{r}U)]+[d_{13}F_2''(z)+d_{14}F_2'(z)-d_{15}F_1''(z)-d_{16}F_1'(z)]e^{-pz}=0 \tag{3.4}$$

Eq. (3.3), can be written in two distinct equations as

$$W''+\frac{1}{r}W'+(d_7P^2+d_6P)W+(d_8P+d_9)\Big(U'+\frac{1}{r}U\Big)+d_{10}\Big(\Phi''+\frac{1}{r}\Phi'\Big)+(d_{12}P^2+d_{11}P)\Phi=0 \tag{3.5}$$

$$d_7F_1''(z)+d_6F_1'(z)+d_{12}F_2''(z)+d_{11}F_2'(z)=0 \tag{3.6}$$

and Eq. (3.4) can be written in two distinct equations as

$$\Phi'' + \frac{1}{r}\Phi' + (d_{13}P^2 + d_{14}P)\Phi - (d_{15}P^2 + d_{16}P)W - d_{17}\Big(W'' + \frac{1}{r}W'\Big) - (d_{18}P + d_{19})\Big(U' + \frac{1}{r}U\Big) = 0 \tag{3.7}$$

$$d_{13}F_2''(z) + d_{14}F_2'(z) - d_{15}F_1''(z) - d_{16}F_1'(z) = 0 \tag{3.8}$$

Eqs. (3.6), (3.8) are a system of homogeneous ordinary differential equations with constant coefficients and the following solution is guessed as

$$F_1(z) = ce^{\Gamma z} \tag{3.9a}$$

$$F_2(z) = \hat{c}e^{\Gamma z} \tag{3.9b}$$

Substituting (3.9) into Eqs. (3.6), (3.8) leads to

$$\begin{bmatrix} d_7\Gamma^2 + d_6\Gamma & d_{12}\Gamma^2 + d_{11}\Gamma \\ -(d_{15}\Gamma^2 + d_{16}\Gamma) & d_{13}\Gamma^2 + d_{14}\Gamma \end{bmatrix} \begin{bmatrix} c \\ \hat{c} \end{bmatrix} = \begin{bmatrix} 0 \\ 0 \end{bmatrix} \tag{3.10}$$

The nontrivial solution to Eq. (3.10) is obtained by setting the determinant of this equation equal to zero as

$$\Gamma^2[(d_7\Gamma + d_6)(d_{13}\Gamma + d_{14}) + (d_{12}\Gamma + d_{11})(d_{15}\Gamma + d_{16})] = 0 \tag{3.11}$$

where

$$d_{20}\Gamma^2 + d_{21}\Gamma + d_{22} = 0 \tag{3.12a}$$

$$\Gamma^2 = 0 \tag{3.12b}$$

coefficients d_{20}, d_{21} and d_{22} in Eq. (3.12a) are given in Appendix. Eq. (3.12) gives

$$\Gamma_{1,2} = \frac{-d_{21} \pm \sqrt{d_{21}^2 - 4d_{20}d_{22}}}{2d_{20}} \tag{3.13a}$$

$$\Gamma_{3,4} = 0 \tag{3.13b}$$

Thus

$$\begin{aligned} F_1(z) &= c_1e^{\Gamma_1 z} + c_2e^{\Gamma_2 z} + c_3 \\ F_2(z) &= d_{23}c_1e^{\Gamma_1 z} + d_{24}c_2e^{\Gamma_2 z} + c_4 \end{aligned} \tag{3.14}$$

Substituting (3.14) into Eq. (3.6), the relation between c and $\hat{c}$ is obtained as

$$\begin{aligned} \hat{c} &= -\frac{d_7\Gamma + d_6}{d_{12}\Gamma + d_{11}}c \\ \hat{c}_1 &= -\frac{d_7\Gamma_1 + d_6}{d_{12}\Gamma_1 + d_{11}}c_1 = d_{23}c_1 \quad \rightarrow \quad d_{23} = -\frac{d_7\Gamma_1 + d_6}{d_{12}\Gamma_1 + d_{11}} \\ \hat{c}_2 &= -\frac{d_7\Gamma_2 + d_6}{d_{12}\Gamma_2 + d_{11}}c_2 = d_{24}c_2 \quad \rightarrow \quad d_{24} = -\frac{d_7\Gamma_2 + d_6}{d_{12}\Gamma_2 + d_{11}} \end{aligned} \tag{3.15}$$

Moreover, Eqs. (3.2), (3.5) and (3.7) are a system of linear homogeneous ordinary differential equations with variable coefficients and the following solution is assumed as

$$U(r) = AJ_1(\beta r) \tag{3.16a}$$

$$W(r) = BJ_0(\beta r) \tag{3.16b}$$

$$\Phi(r) = CJ_0(\beta r) \tag{3.16c}$$

Substituting (3.14) and (3.16) into Eq. (3.1) leads to

$$u_{(r,z)} = AJ_1(\beta r)e^{pz} \tag{3.17a}$$

$$w_{(r,z)} = BJ_0(\beta r)e^{pz} + C_1e^{\Gamma_1 z} + C_2e^{\Gamma_2 z} + C_3 \tag{3.17b}$$

$$\phi_{(r,z)} = CJ_0(\beta r)e^{pz} + d_{23}C_1e^{\Gamma_1 z} + d_{24}C_2e^{\Gamma_2 z} + C_4 \tag{3.17c}$$

Substituting (3.17a), (3.17b) and (3.17c) into Eqs. (3.2), (3.5) and (3.7) results in

$$\{[-\beta^2+(d_2P^2+d_1P)]A-[B(d_3P+d_1)+C(d_4P+d_5)]\beta\}J_1(\beta r)=0 \tag{3.18a}$$

$$\{[-\beta^2+(d_7P^2+d_6P)]B+A\beta(d_8P+d_9)+[-\beta^2d_{10}+(d_{12}P^2+d_{11}P)]C\}J_0(\beta r)=0 \tag{3.18b}$$

$$\{[-\beta^2+(d_{13}P^2+d_{14}P)]C+[\beta^2d_{17}-(d_{15}P^2+d_{16}P)]B-\beta(d_{18}P+d_{19})A\}J_0(\beta r)=0 \tag{3.18c}$$

Eqs. (3.18) show that (3.17a), (3.17b) and (3.17c) can be the solutions to the system of Eqs. (3.2), (3.5) and (3.7) if and only if

(3.19)
$$\begin{bmatrix} -\beta^2+(d_2P^2+d_1P) & -\beta(d_3P+d_1) & -\beta(d_4P+d_5) \\ \beta(d_8P+d_9) & -\beta^2+(d_7P^2+d_6P) & -\beta d_{10}+(d_{12}P^2+d_{11}P) \\ -\beta(d_{18}P+d_{19}) & \beta^2d_{17}-(d_{15}P^2+d_{16}P) & -\beta^2+(d_{13}P^2+d_{14}P) \end{bmatrix} \begin{bmatrix} A \\ B \\ C \end{bmatrix} = \begin{bmatrix} 0 \\ 0 \\ 0 \end{bmatrix}$$

The nontrivial solution to Eq. (3.19) is obtained by setting the determinant of this equation equal to zero as

$$\begin{aligned} &(a_{11}\cdot a_{22}\cdot a_{33}) + (a_{12}\cdot a_{23}\cdot a_{31}) + (a_{13}\cdot a_{21}\cdot a_{32}) \\ &\quad - (a_{13}\cdot a_{22}\cdot a_{31}) - (a_{12}\cdot a_{21}\cdot a_{33}) - (a_{11}\cdot a_{23}\cdot a_{32}) = 0 \end{aligned} \tag{3.20}$$

Eq. (3.20) is a six order polynomial in term p; it gives six roots P_1–P_6 and coefficients a_{ij} in Eq. (3.20) which are given in Appendix. Additionally, Eq. (3.19) gives a relation between A and B, as well as A and C. So

$$B_m = N_m \cdot A_m \qquad C_m = M_m \cdot A_m \tag{3.21}$$

where

$$N_m = \frac{a_{13}a_{21} - a_{11}a_{23}}{a_{12}a_{23} - a_{13}a_{22}} \qquad M_m = \frac{a_{12}a_{21} - a_{11}a_{22}}{a_{13}a_{22} - a_{12}a_{23}} \tag{3.22}$$

Application of the homogeneous boundary conditions. We assume zero displacement in radial direction at $r = a$

$$u(a,z) = 0 \quad \rightarrow \quad J_1(\beta a) = 0 \tag{3.23}$$

Eq. (3.23) gives infinite roots for β_m. It needs to be noted that Eq. (3.20) gives six values of $P(P_{1m}$ to $P_{6m})$ for each β. The boundary conditions in axial direction at

$r = a$ are assumed to be

$$w(a,0) = w(a,h) = 0 \tag{3.24a}$$

$$\phi(a,0) = \phi(a,h) = 0 \tag{3.24b}$$

The application of boundary condition (3.24a) to Eq. (3.17) leads to the following equations:

$$\begin{aligned} J_0(\beta_m a)[&A_{1m}N_{1m} + A_{2m}N_{2m} + A_{3m}N_{3m} + A_{4m}N_{4m} \\ &+ A_{5m}N_{5m} + A_{6m}N_{6m}] + C_{1m} + C_{2m} + C_{3m} = 0 \end{aligned} \tag{3.25a}$$

$$\begin{aligned} J_0(\beta_m a)[&A_{1m}N_{1m}e^{P_{1m}h} + A_{2m}N_{2m}e^{P_{2m}h} + A_{3m}N_{3m}e^{P_{3m}h} + A_{4m}N_{4m}e^{P_{4m}h} \\ &+ A_{5m}N_{5m}e^{P_{5m}h} + A_{6m}N_{6m}e^{P_{6m}h}] + C_{1m}e^{\Gamma_1 h} + C_{2m}e^{\Gamma_2 h} + C_{3m} = 0 \end{aligned} \tag{3.25b}$$

$$\begin{aligned} J_0(\beta_m a)[&A_{1m}M_{1m} + A_{2m}M_{2m} + A_{3m}M_{3m} + A_{4m}M_{4m} \\ &+ A_{5m}M_{5m} + A_{6m}M_{6m}] + d_{23}C_{1m} + d_{24}C_{2m} + C_{4m} = 0 \end{aligned} \tag{3.25c}$$

$$\begin{aligned} J_0(\beta_m a)[&A_{1m}M_{1m}e^{P_{1m}h} + A_{2m}M_{2m}e^{P_{2m}h} + A_{3m}M_{3m}e^{P_{3m}h} + A_{4m}M_{4m}e^{P_{4m}h} \\ &+ A_{5m}M_{5m}e^{P_{5m}h} + A_{6m}M_{6m}e^{P_{6m}h}] + d_{23}C_{1m}e^{\Gamma_1 h} + d_{24}C_{2m}e^{\Gamma_2 h} + C_{4m} = 0 \end{aligned} \tag{3.25d}$$

The constant coefficients d_{25} to d_{28} are given in Appendix. Considering the fact that there is an infinite number of β_m, there will be an infinite number of C_1 and C_2 as C_{1m} and C_{2m}, respectively:

$$\begin{bmatrix} 1 - e^{\Gamma_1 h} & 1 - e^{\Gamma_2 h} \\ (1 - e^{\Gamma_1 h})d_{23} & (1 - e^{\Gamma_2 h})d_{24} \end{bmatrix} \begin{bmatrix} C_{1m} \\ C_{2m} \end{bmatrix} = \begin{bmatrix} d_{26} - d_{25} \\ d_{28} - d_{27} \end{bmatrix} \tag{3.26}$$

Thus

$$C_{1m} = \frac{(d_{26} - d_{25})(d_{24} - d_{23}) - (d_{28} - d_{27}) + d_{23}(d_{26} - d_{25})}{(1 - e^{\Gamma_1 h})(d_{24} - d_{23})}$$

$$C_{2m} = \frac{(d_{28} - d_{27}) - d_{23}(d_{26} - d_{25})}{(1 - e^{\Gamma_2 h})(d_{24} - d_{23})}$$

By substituting C_{1m}, C_{2m} and the constant coefficients d_{25} to d_{28} into Eqs. (3.25a) and (3.25c), the values of C_{3m} and C_{4m} are obtained. Finally, the solution to the Navier equations will be

$$\begin{aligned} u(r,z) = \sum_{m=1}^{\infty} J_1(\beta_m r)[&A_{1m}e^{P_{1m}z} + A_{2m}e^{P_{2m}z} + A_{3m}e^{P_{3m}z} \\ &+ A_{4m}e^{P_{4m}z} + A_{5m}e^{P_{5m}z} + A_{6m}e^{P_{6m}z}] \end{aligned} \tag{3.27a}$$

$$\begin{aligned} w(r,z) = \sum_{m=1}^{\infty} J_0(\beta_m r)[&A_{1m}N_{1m}e^{P_{1m}z} + A_{2m}N_{2m}e^{P_{2m}z} \\ &+ A_{3m}N_{3m}e^{P_{3m}z} + A_{4m}N_{4m}e^{P_{4m}z} + A_{5m}N_{5m}e^{P_{5m}z} \\ &+ A_{6m}N_{6m}e^{P_{6m}z}] + C_{1m}e^{\Gamma_1 z} + C_{2m}e^{\Gamma_2 Z} + C_{3m} \end{aligned} \tag{3.27b}$$

$$\begin{aligned}(3.27c)\quad \phi(r,z) = \sum_{m=1}^{\infty} J_0(\beta_m r)[&A_{1m}M_{1m}e^{P_{1m}z} + A_{2m}M_{2m}e^{P_{2m}z} \\ &+ A_{3m}M_{3m}e^{P_{3m}z} + A_{4m}M_{4m}e^{P_{4m}z} + A_{5m}M_{5m}e^{P_{5m}z} \\ &+ A_{6m}M_{6m}e^{P_{6m}z}] + d_{23}C_{1m}e^{\Gamma_1 z} + d_{24}C_{2m}e^{\Gamma_2 Z} + C_{4m}\end{aligned}$$

Remaining coefficients A_{im} will be indicated using boundary conditions in z direction. We assume the most general boundary conditions on the upper and lower surfaces of the plate as

$$\begin{aligned}K_{11}\Big[u_{,r}(r,0) + \frac{1}{r}u(r,0)\Big] + K_{12}w(r,0) + K_{13}w_{,z}(r,0) \\ +K_{14}T(r,0) + K_{15}\phi_z(r,0) = S_1(r) \\ K_{21}u(r,0) + K_{22}u_{,z}(r,0) + K_{23}w_{,r}(r,0) + K_{24}\phi_r(r,0) = S_2(r) \\ K_{31}\Big[u_{,r}(r,h) + \frac{1}{r}u(r,h)\Big] + K_{32}w(r,h) + K_{33}w_{,z}(r,h) \\ +K_{34}T(r,h) + K_{35}\phi_z(r,h) = S_3(r) \\ K_{41}u(r,h) + K_{42}u_{,z}(r,h) + K_{43}w_{,r}(r,h) + K_{44}\phi_r(r,h) = S_4(r) \\ K_{51}\phi(r,0) + K_{52}\phi_z(r,0) = S_5(r) \\ K_{61}\phi(r,h) + K_{62}\phi_z(r,h) = S_6(r)\end{aligned} \tag{3.28}$$

where K_{ij} are constants; by assigning different values to them, different types of boundary conditions may be obtained; $S_i(r)$ are known functions. Substituting Eqs. (3.28) into Eqs. (2.5), (2.6) and (2.7), the stresses and electric displacements are obtained.

4. Results and discussion

As shown in Figure 2, a circular thick disk of radius "a" and thickness "h" is made of undrained porous piezoelectric hexagonal material symmetry of class 6 mm, whose properties are shown in Table 1. Mainly to simulate practical problems, the upper surface of the plate is partially exposed to mechanical load varying with the linear law, $P(r) = \sigma_{zz} = -P_0 r$; $P_0 = 100$ MPa. Shear stress is considered zero on the upper and lower surfaces. Moreover, the axial normal stress is considered zero on the lower surface. The boundary is assumed to be fixed such that the mechanical boundary condition at radius a is $u(a,z) = 0$, and axial displacement in the boundary surface is limited at the upper and lower band, $w(a,0) = 0$ and $w(a,h) = 0$.

Material constants are considered for a cadmium selenide plate which possesses class 6 mm symmetry [7] as shown in Table 1.

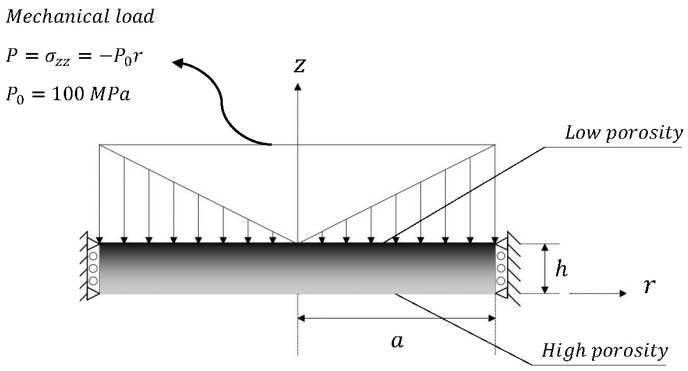

FIGURE 2. Geometry of a piezoelectric poroelastic circular thick disk under the mechanical load and boundary conditions

TABLE 1

Parameter	Numerical
c_{11}	74.1 GPa
c_{12}	45.2 GPa
c_{13}	45.2 GPa
c_{22}	74.1 GPa
c_{55}	16.2 GPa
E_0	107 GPa
γ	0.75
e_{15}	$-0.138\left(\frac{C}{m^2}\right)$
v	0.2
v_u	0.3
η_{11}	$82.6 \times 10^{-12}\left(\frac{C^2}{N \cdot m^2}\right)$
η_{33}	$90.3 \times 10^{-12}\left(\frac{C^2}{N \cdot m^2}\right)$
e_{31}	$-0.160\left(\frac{C}{m^2}\right)$
e_{32}	$-0.160\left(\frac{C}{m^2}\right)$
e_{33}	$0.347\left(\frac{C}{m^2}\right)$

Results for this problem are shown in Figures 3 to 20.

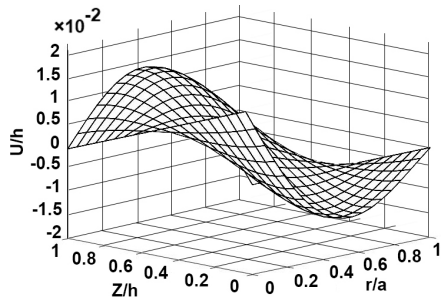

(a)

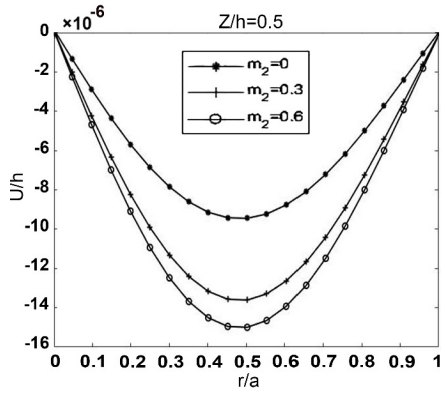

(b)

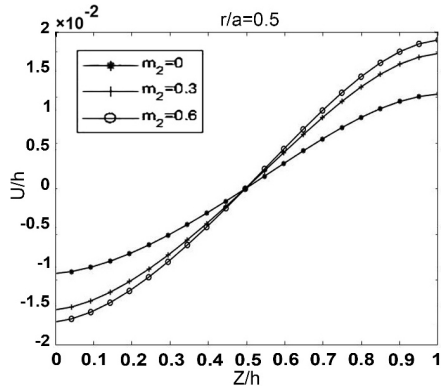

(c)

FIGURE 3. (a) Radial displacement in the cross section of circular thick disk; (b) radial displacement versus r/a at $z/h = 0.5$;(c) radial displacement versus z/h at $r/a = 0.5$

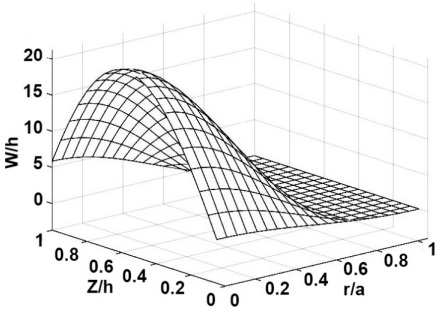

(a)

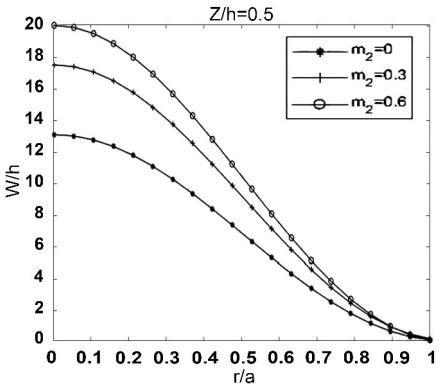

(b)

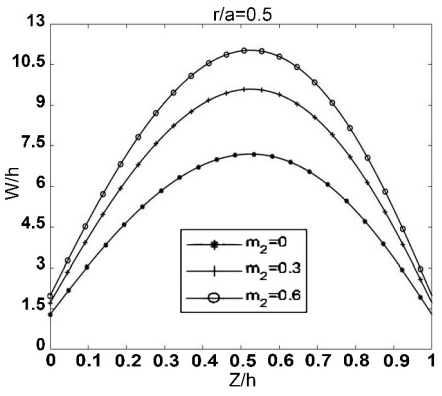

(c)

FIGURE 4. (a) Axial displacement in the cross section of a circular thick disk; (b) axial displacement versus r/a at $z/h = 0.5$;(c) axial displacement versus z/h at $r/a = 0.5$

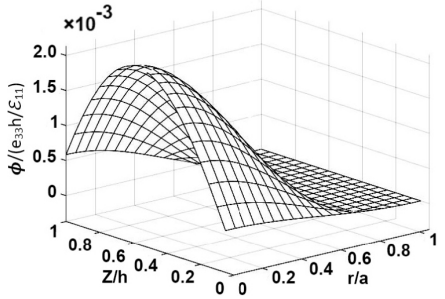

(a)

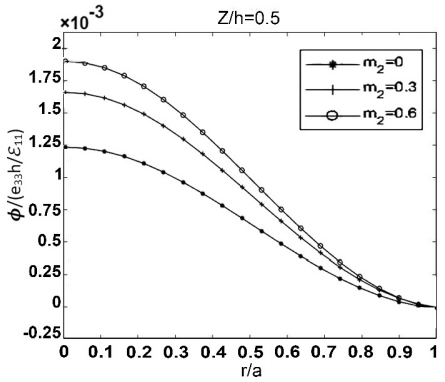

(b)

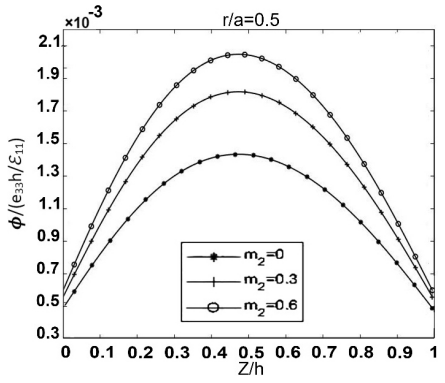

(c)

FIGURE 5. (a) Electric potential in the cross section of a circular thick disk; (b) electric potential versus r/a at $z/h = 0.5$; (c) electric potential versus z/h at $r/a = 0.5$

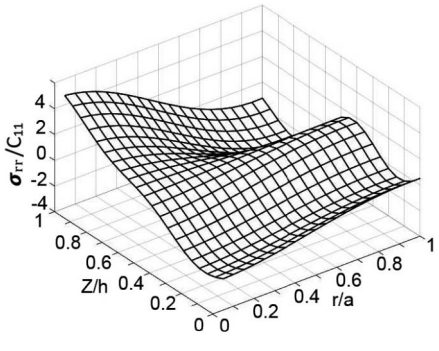

(a)

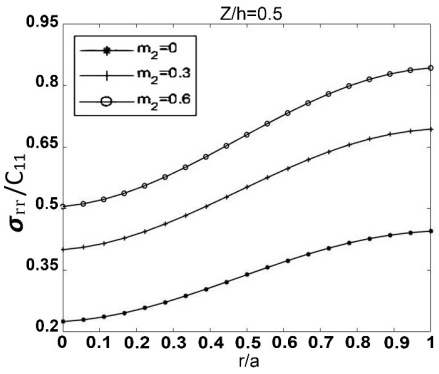

(b)

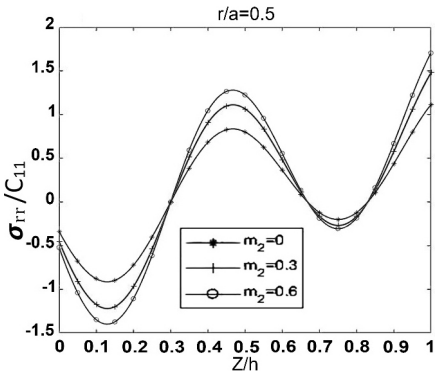

(c)

FIGURE 6. (a) Radial mechanical stress in the cross section of a circular thick disk; (b) distribution of radial mechanical stress versus r/a at $z/h = 0.5$; (c) distribution of radial mechanical stress versus z/h at $r/a = 0.5$

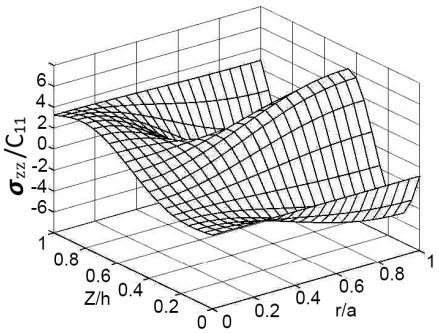

(a)

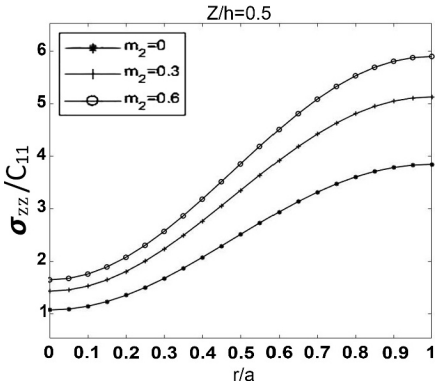

(b)

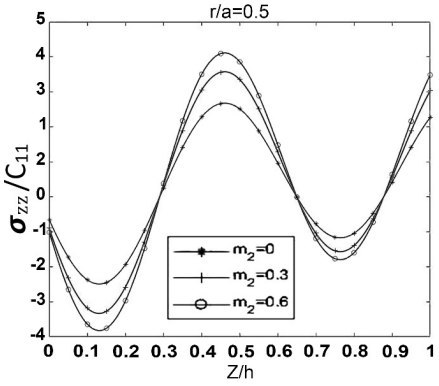

(c)

FIGURE 7. (a) Axial mechanical stress in the cross section of a circular thick disk; (b) distribution of axial mechanical stress versus r/a at $z/h = 0.5$; (c) distribution of axial mechanical stress versus z/h at $r/a = 0.5$

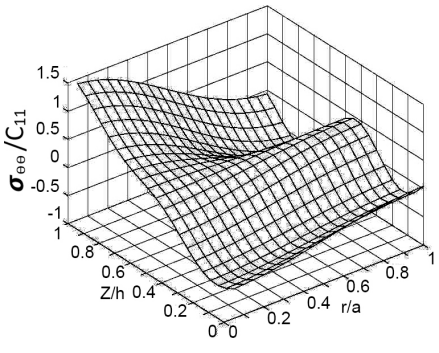

(a)

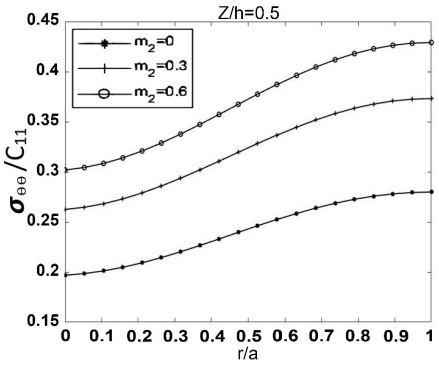

(b)

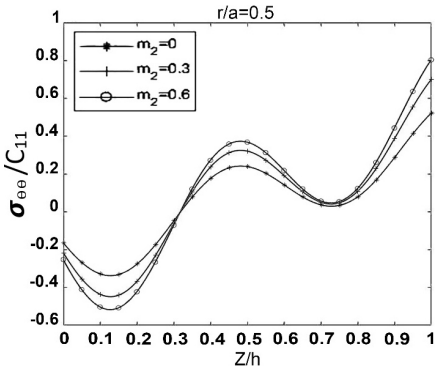

(c)

FIGURE 8. (a) Hoop mechanical stress in the cross section of a circular thick disk; (b) distribution of hoop mechanical stress versus r/a at $z/h = 0.5$; (c) distribution of hoop mechanical stress versus z/h at $r/a = 0.5$

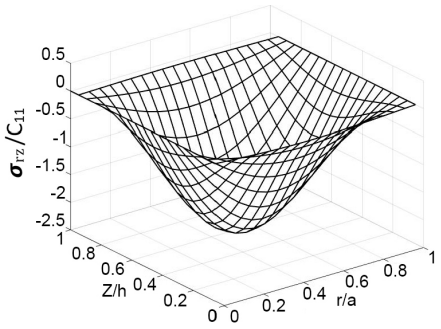

(a)

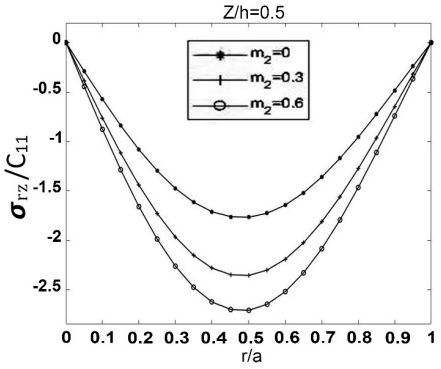

(b)

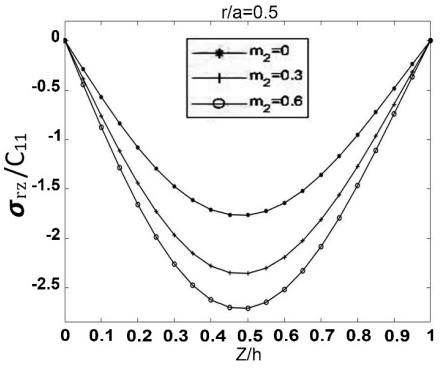

(c)

FIGURE 9. (a)Shear mechanical stress in the cross section of circular thick disk;(b)distribution of shear mechanical stress versus r/a at $z/h = 0.5$;(c)distribution of shear mechanical stress versus z/h at $r/a = 0.5$

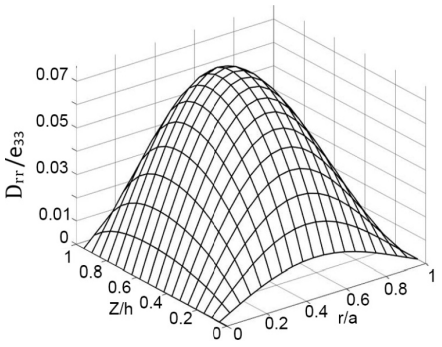

(a)

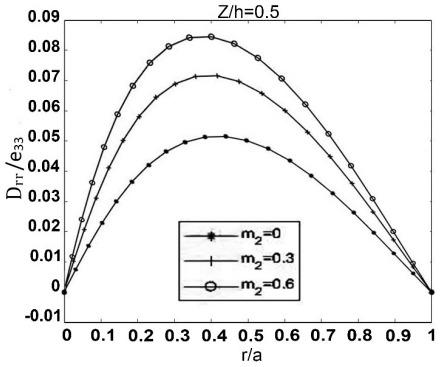

(b)

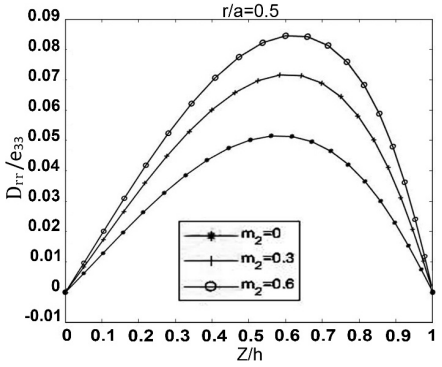

(c)

FIGURE 10. (a) Radial electric displacement in the cross section of a circular thick disk; (b) variation of radial electric displacement versus r/a at $z/h = 0.5$; (c) variation of radial electric displacement versus z/h at $r/a = 0.5$

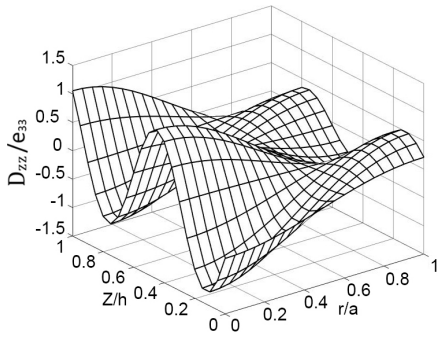

(a)

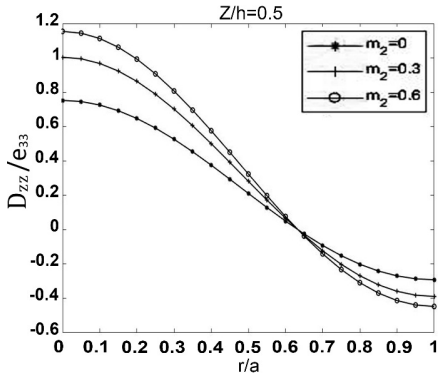

(b)

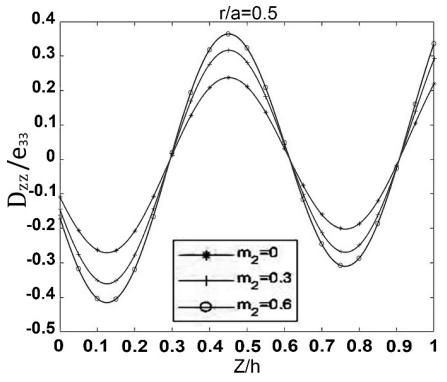

(c)

FIGURE 11. (a) Axial electric displacement in the cross section of a circular thick disk; (b) variation of axial electric displacement versus r/a at $z/h = 0.5$; (c) variation of axial electric displacement versus z/h at $r/a = 0.5$

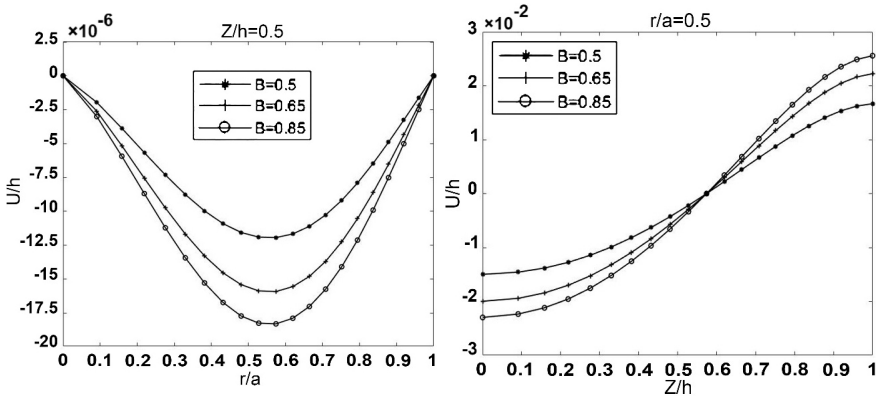

(a) (b)

FIGURE 12. (a) Radial displacement versus r/a at $z/h = 0.5$ for different values of the compressibility coefficient B; (b) radial displacement versus z/h at $r/a = 0.5$ for different values of the compressibility coefficient B

Here, B is a compressibility coefficient, sometimes called the Skempton pore pressure coefficient, which is related to poisson's ratio, and undrained poisson's ratio. The under undrained condition as

$$B = \frac{(3\nu_u - \nu)}{(1 - 2\nu)(1 + \nu_u)}, \qquad 0 \leqslant B \leqslant 1 \tag{4.1}$$

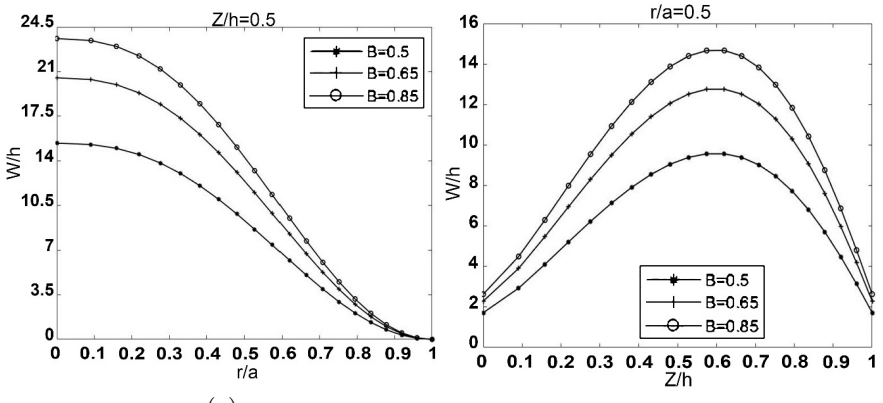

(a) (b)

FIGURE 13. (a) Axial displacement versus r/a at $z/h = 0.5$ for different values of the compressibility coefficient; (b) axial displacement versus z/h at $r/a = 0.5$ for different values of the compressibility coefficient

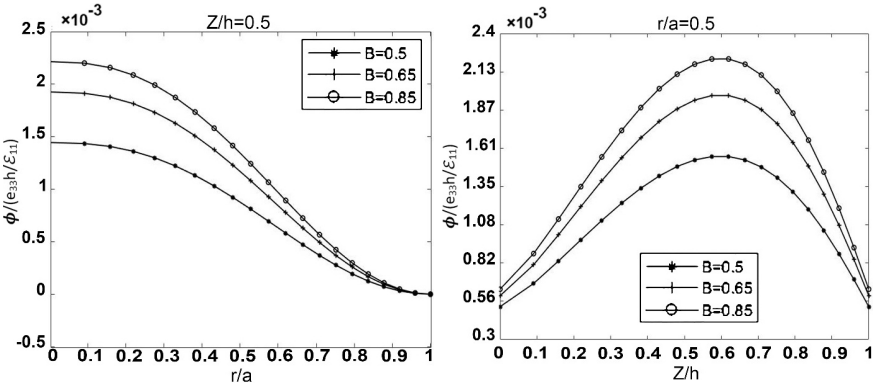

(a) (b)

FIGURE 14. (a) Electric potential versus r/a at $z/h = 0.5$ for different values of the compressibility coefficient; (b) electric potential versus z/h at $r/a = 0.5$ for different values of the compressibility coefficient

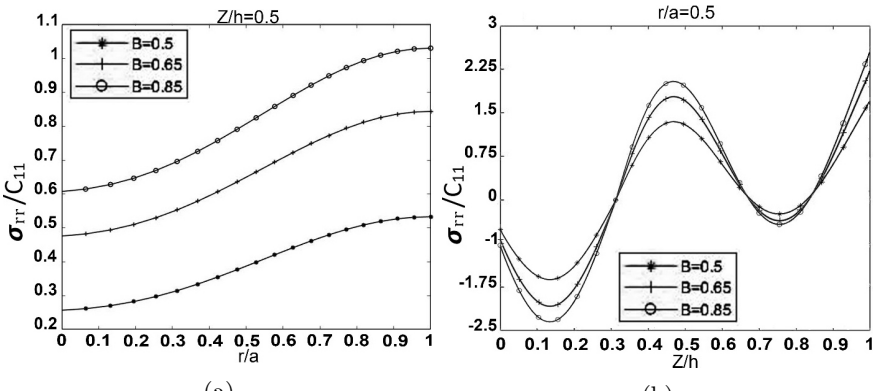

(a) (b)

FIGURE 15. (a) Radial mechanical stress versus r/a at $z/h = 0.5$ for different values of the compressibility coefficient; (b) radial mechanical stress versus z/h at $r/a = 0.5$ for different values of the compressibility coefficient

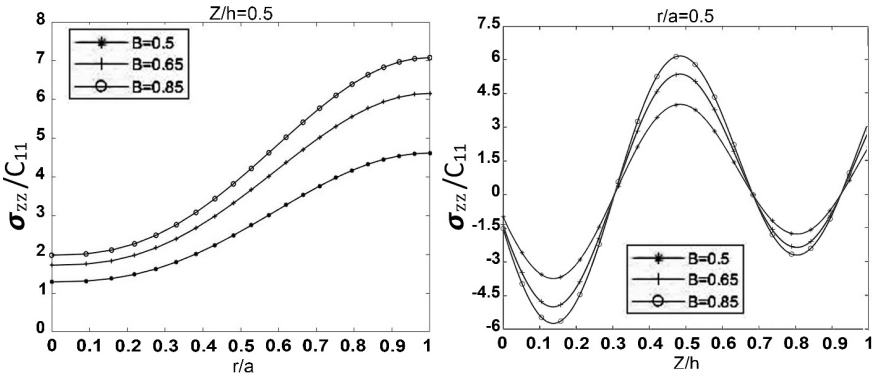

(a) (b)

FIGURE 16. (a) Axial mechanical stress versus r/a at $z/h = 0.5$ for different values of the compressibility coefficient; (b) axial mechanical stress versus z/h at $r/a = 0.5$ for different values of the compressibility coefficient

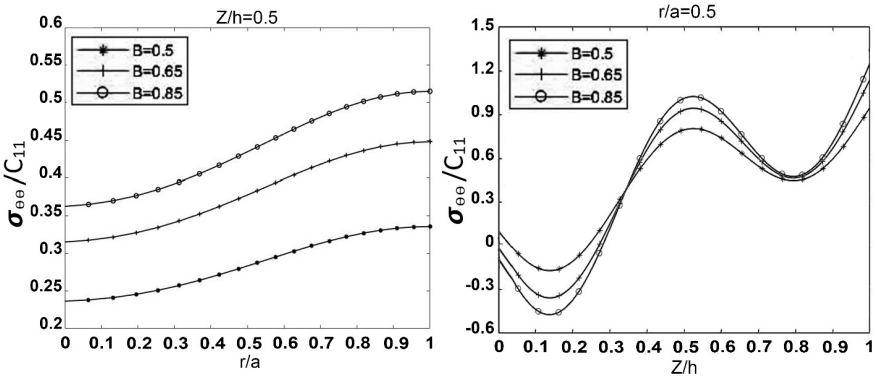

(a) (b)

FIGURE 17. (a) Hoop mechanical stress versus r/a at $z/h = 0.5$ for different values of the compressibility coefficient; (b) hoop mechanical stress versus z/h at $r/a = 0.5$ for different values of the compressibility coefficient

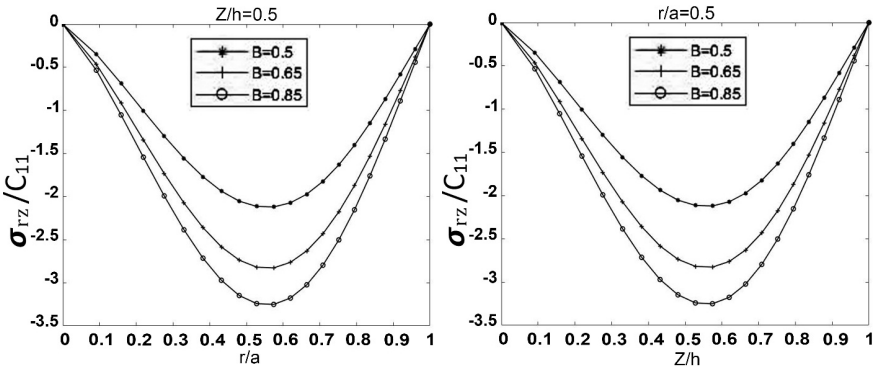

(a) (b)

FIGURE 18. (a) Shear mechanical stress versus r/a at $z/h = 0.5$ for different values of the compressibility coefficient; (b) shear mechanical stress versus z/h at $r/a = 0.5$ for different values of the compressibility coefficient

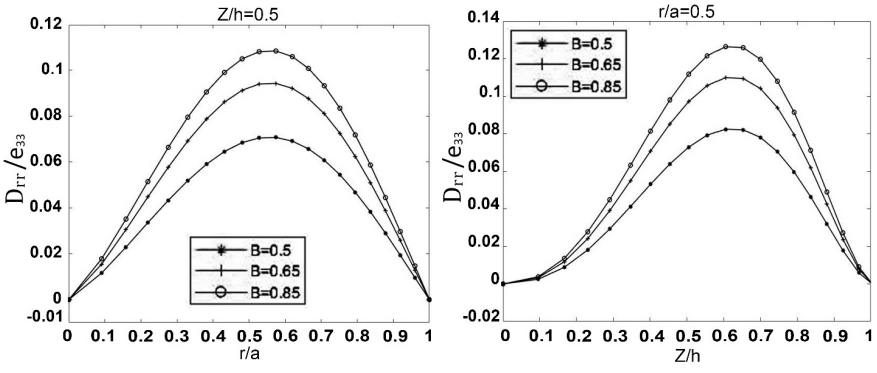

(a) (b)

FIGURE 19. (a) Radial electric displacement versus r/a at $z/h = 0.5$ for different values of the compressibility coefficient; (b) radial electric displacement versus z/h at $r/a = 0.5$ for different values of the compressibility coefficient

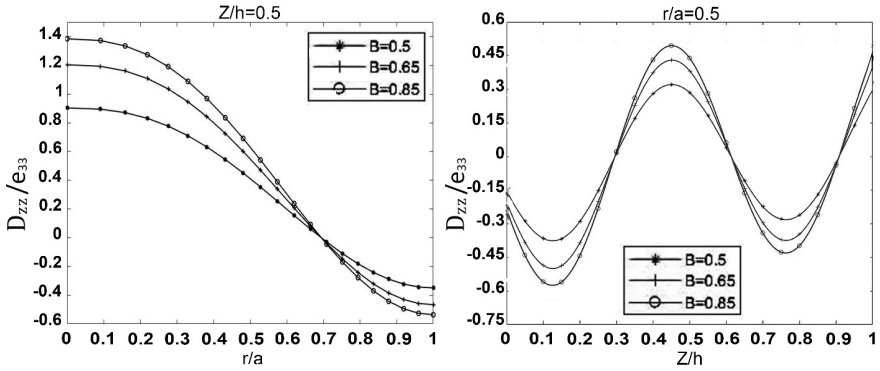

(a) (b)

FIGURE 20. (a) Axial electric displacement versus r/a at $z/h = 0.5$ for different values of the compressibility coefficient; (b) axial electric displacement versus z/h at $r/a = 0.5$ for different values of the compressibility coefficient

The suggested solutions for displacement, electric potential, and stress field are of the series form and by summing up 30 successive terms have a truncation error of the order of 10^{-5}. Figure 3a shows the resulting radial displacement due to mechanical load. The radial displacement versus r/a is shown in Figure 3b. The maximum radial displacement falls in half of the radius and it is zero at the center due to the axisymmetric condition of the problem. Figure 3c shows the radial displacement varying in axial direction. The considerable point is that for different values of m_2 there is a unique zero displacement point which is somewhere between 0.45 and 0.55 of dimensionless thickness; this point is interestingly the location of the neutral axis. Figure 4a shows the resulting axial displacement caused by mechanical load. Figure 4b shows the axial displacement varying in radial direction, where the maximum deflection, due to mechanical load, is in the center of the plate and it is zero at the outer radius of the plate where we imposed a supported boundary condition. Axial displacement versus z/h is shown in Figure 4c. The maximum axial displacement occurs near the dimensionless thickness of 0.5. Figure 5a demonstrates the resulting electric potential related to the mechanical load. The electric potential versus r/a is shown in Figure 5b. It shows that the maximum electric potential falls in the center of the plate and that it is zero at $r/a = 1$ due to the axisymmetric condition of the problem. Figure 5c indicates that the electric potential varies in axial direction and that it is maximum near the dimensionless thickness of 0.5. Figures 6a, 7a, 8a and 9a show the radial, axial, circumferential, and shear mechanical stresses in the cross section of the circular thick disk, respectively. Figures 6b, 7b, 8b and 9b are the plots of stresses versus r/a at $z/h = 0.5$. It is shown that as m_2 increases so do the radial, axial, hoop, and shear mechanical stresses. Figures 6c, 7c and 8c show that the radial, axial, and circumferential mechanical stresses follow a harmonic pattern along the dimensionless thickness. The

shear mechanical stress versus z/h is shown in Figure 9c. It shows that the maximum shear stress is near the dimensionless thickness of 0.5. The resulting radial and axial electric displacements D_{rr} and D_{zz} are shown in Figures 10a and 11a, respectively. Figure 10b indicates that the maximum D_{rr} displacement falls in $r/a = 0.4$. Moreover, it is shown that as m_2 increases so does the radial electric displacement. It is noted that, due to the assumed boundary conditions, D_{rr} is zero at $r/a = 0$ and $r/a = 1$. Figure 10c shows the radial electric displacement versus z/h. It is shown that the maximum D_{rr} falls in $z/h = 0.6$. Figure 11b shows that the maximum D_{zz} displacement falls in $r/a = 0$ and $r/a = 1$. Moreover, it is zero in $r/a = 0.6$. Figure 11c demonstrates that as m_2 increases, the axial electric displacement also increases. Figures 12a, 13a and 14a present the distribution of the radial and axial displacements and the electric potential along the radius for different values of the pore compressibility coefficient B. Figures 12b, 13b and 14b also show the distribution of these displacements and the electric potential along the thickness, respectively, for different values of the pore compressibility coefficient B. Figures 15a, 16a, 17a and 18a demonstrate the distribution of the radial, axial, hoop, and shear mechanical stresses along the radius, respectively, where the pore compressibility coefficient B is changed and the other parameters are fixed. Figures 15b, 16b, 17b and 18b show the distribution of the same stresses along the thickness, for different values of the pore compressibility coefficient B. Figures 19a and 20a present the variation of the radial and axial electric displacements along the radius where the pore compressibility coefficient B is changed and the other parameters are fixed. Figures 19b and 20b indicate the variation of the same electric displacements along the thickness, for different values of the pore compressibility coefficient B.

5. Conclusions

This paper presents an analytical solution for the calculation of the axisymmetric mechanical stresses in a piezoelectric poroelastic circular thick disk. The material properties through the porous direction are assumed to be nonlinear with an exponential law distribution. The mechanical stresses are obtained through the direct method of solution for the Navier equation. In the present study, a linear varying distributed external axisymmetric mechanical load acts on the plate and the boundary is assumed to be fixed. It is concluded that:

(i) The neutral axis and plane of the plate will not fall in the midsurface.
(ii) Greater m_2 will pass the neutral axis far from the mid-plane of the plate.
(iii) Axial and radial displacement through the thickness and radius of the plate is not constant and linear.
(iv) Radial displacement in radial direction is affected considerably near the center of the plate.
(v) Electric potential through the thickness and radius of the plate is not constant and linear.
(vi) It is interesting to see that except for the shear stress other stresses follow a harmonic pattern along the thickness of the plate due to mechanical loads.

(vii) There is a zero point for the radial, axial and circumferential mechanical stresses across the thickness which is near 0.3 of the dimensionless thickness. Because of the porosity distribution profile, this point is the neutral axis of the plate.

(viii) Axial electric displacement follows a harmonic pattern along the dimensionless thickness.

Appendix A.

$$d_1 = \frac{\overline{c^*}_{55}}{\overline{c^*}_{11}}\frac{m}{h} \qquad d_2 = \frac{\overline{c^*}_{55}}{\overline{c^*}_{11}} \qquad d_3 = \frac{\overline{c^*}_{13}+\overline{c^*}_{55}}{\overline{c^*}_{11}} \qquad d_4 = \frac{\overline{e}_{31}+\overline{e}_{15}}{\overline{c^*}_{11}}$$

$$d_5 = \frac{\overline{e}_{15}}{\overline{c^*}_{11}}\frac{m}{h} \qquad d_6 = \frac{\overline{c^*}_{33}}{\overline{c^*}_{55}}\frac{m}{h} \qquad d_7 = \frac{\overline{c^*}_{33}}{\overline{c^*}_{55}} \qquad d_8 = \frac{\overline{c^*}_{13}}{\overline{c^*}_{55}} + 1$$

$$d_9 = \frac{\overline{c^*}_{13}}{\overline{c^*}_{55}}\frac{m}{h} \qquad d_{10} = \frac{\overline{e}_{15}}{\overline{c^*}_{55}} \qquad d_{11} = \frac{\overline{e}_{33}}{\overline{c^*}_{55}}\frac{m}{h} \qquad d_{12} = \frac{\overline{e}_{33}}{\overline{c^*}_{55}}$$

$$d_{13} = \frac{\overline{\eta}_{33}}{\overline{\eta}_{11}} \qquad d_{14} = \frac{\overline{\eta}_{33}}{\overline{\eta}_{11}}\frac{m}{h} \qquad d_{15} = \frac{\overline{e}_{33}}{\overline{\eta}_{11}} \qquad d_{16} = \frac{\overline{e}_{33}}{\overline{\eta}_{11}}\frac{m}{h}$$

$$d_{17} = \frac{\overline{e}_{15}}{\overline{\eta}_{11}} \qquad d_{18} = \frac{\overline{e}_{15}+\overline{e}_{31}}{\overline{\eta}_{11}} \qquad d_{19} = \frac{\overline{e}_{31}}{\overline{\eta}_{11}}\frac{m}{h} \qquad d_{20} = d_7 d_{13} + d_{12} d_{15}$$

$$d_{21} = d_7 d_6 + d_6 d_{13} + d_{12} d_{16} + d_{11} d_{15} \qquad d_{22} = d_6 d_{14} + d_{11} d_{16}$$

$$\begin{aligned}
a_{11} &= -\beta^2 + (d_2 P^2 + d_1 P)\\
a_{12} &= -\beta(d_3 P + d_1)\\
a_{13} &= -\beta(d_4 P + d_5)\\
a_{21} &= \beta(d_8 P + d_9)\\
a_{22} &= -\beta^2 + (d_7 P^2 + d_6 P)\\
a_{23} &= -\beta d_{10} + (d_{12} P^2 + d_{11} P)\\
a_{31} &= -\beta(d_{18} P + d_{19})\\
a_{32} &= \beta^2 d_{17} - (d_{15} P^2 + d_{16} P)\\
a_{33} &= -\beta^2 + (d_{13} P^2 + d_{14} P)
\end{aligned}$$

$$d_{25} = J_0(\beta_m a)\big[A_{1m}N_{1m} + A_{2m}N_{2m} + A_{3m}N_{3m} + A_{4m}N_{4m} + A_{5m}N_{5m} + A_{6m}N_{6m}\big]$$

$$\begin{aligned}
d_{26} = J_0(\beta_m a)\big[&A_{1m}N_{1m}e^{P_{1m}h} + A_{2m}N_{2m}e^{P_{2m}h} + A_{3m}N_{3m}e^{P_{3m}h}\\
&+ A_{4m}N_{4m}e^{P_{4m}h} + A_{5m}N_{5m}e^{P_{5m}h} + A_{6m}N_{6m}e^{P_{6m}h}\big]
\end{aligned}$$

$$d_{27} = J_0(\beta_m a)\big[A_{1m}M_{1m} + A_{2m}M_{2m} + A_{3m}M_{3m} + A_{4m}M_{4m} + A_{5m}M_{5m} + A_{6m}M_{6m}\big]$$

$$\begin{aligned}
d_{28} = J_0(\beta_m a)\big[&A_{1m}M_{1m}e^{P_{1m}h} + A_{2m}M_{2m}e^{P_{2m}h} + A_{3m}M_{3m}e^{P_{3m}h}\\
&+ A_{4m}M_{4m}e^{P_{4m}h} + A_{5m}M_{5m}e^{P_{5m}h} + A_{6m}M_{6m}e^{P_{6m}h}\big]
\end{aligned}$$

Acknowledgments. We would like to express our gratitude to the Islamic Azad University, South Tehran Branch, Tehran, Iran for its support of the PhD research project of Ali Abjadi entitled "Thermal stress analysis of a piezo-poroelastic circular plate".

References

1. A. B. Dobrucki, P. Pruchnicki, *Theory of piezoelectric axisymmetric bimorph*, Sensors and Actuators A: Physical **58**(3) (1997), 203–212.
2. H. J. Ding, H. M. Wang, P. F. Hou, *The transient responses of piezoelectric hollow cylinders for axisymmetric plane strain problems*, Int. J. Solids Struct. **40**(1) (2003), 105–123.
3. W. Zi-kung, C. Geng-chao, *A general solution and the application of space axisymmetric problem in piezoelectric material*, Appl. Math. Mech. **15**(7) (1994), 615–626.
4. S. Kapuria, S. Sengupta, P. C. Dumir, *Three-dimensional solution for simply-supported piezoelectric cylindrical shell for axisymmetric load*, Comput. Methods Appl. Mech. Eng. **140**(1) (1997), 139–155.
5. N. Kharouf, P. R. Heyliger, *Axisymmetric free vibrations of homogeneous and laminated piezoelectric cylinders*, J. Sound Vib. **174**(4) (1994), 539–561.
6. F. Ebrahimi, A. Rastgoo, M. H. Kargarnovin, *Analytical investigation on axisymmetric free vibrations of moderately thick circular functionally graded plate integrated with piezoelectric layers*, Journal of Mechanical Science and Technology **22**(6) (2008), 1058–1072.
7. F. Ashida, T. R. Tauchert, *Transient response of a piezothermoelastic circular disk under axisymmetric heating*, Acta Mech. **128**(1) (1998), 1–14.
8. S. Kapuria, S. Sengupta, P. C. Dumir, *Three-dimensional solution for a hybrid cylindrical shell under axisymmetric thermoelectric load*, Arch. Appl. Mech. **67**(5) (1997), 320–330.
9. J. Sladek, V. Sladek, P. Solek, A. Saez, *Dynamic 3D axisymmetric problems in continuously non-homogeneous piezoelectric solids*, Int. J. Solids Struct. **45**(16) (2008), 4523–4542.
10. S. Dong, K. Uchino, L. Li, D. Viehland, *Analytical solutions for the transverse deflection of a piezoelectric circular axisymmetric unimorph actuator*, IEEE Transactions on Ultrasonics, Ferroelectrics, and Frequency Control **54**(6) (2007), 1240–1249.
11. W. X. Zhang, H. Wang, *Axisymmetric boundary condition problems for transversely isotropic piezoelectric materials*, Mech. Res. Commun. **87** (2018), 7–12.
12. P. Zhang, J. Liu, G. Lin, *Axisymmetric solutions for the multi-layered transversely isotropic piezoelectric medium*, Appl. Math. Comput. **290** (2016), 355–375.
13. S. S. Volkov, A. S. Vasiliev, S. M. Aizikovich, B. I. Mitrin, *Axisymmetric indentation of an electroelastic piezoelectric half-space with functionally graded piezoelectric coating by a circular punch*, Acta Mech. **230**(4) (2019), 1289–1302.
14. M. Ishihara, Y. Ootao, Y. Kameo, T. Saito, *Thermoelectroelastic response of a piezoelectric cylinder with D symmetry under axisymmetric mechanical and thermal loading*, Mechanical Engineering Journal **4**(5) (2008), 16-00609.
15. J. Liu, P. Zhang, G. Lin, Gao C. Li, S. Lu, *Elastostatic solutions of a multilayered transversely isotropic piezoelectric system under axisymmetric loading*, Acta Mech. **228**(1) 2017, 107–128.
16. T-J. Liu, C. Zhang, Y-S. Wang, *Analysis of axisymmetric indentation of functionally graded piezoelectric coating or substrate systems under an insulator indenter*, Journal of Intelligent Material Systems and Structures **28**(1) (2017), 23–34.
17. X. Zhao, X. Y. Li, Y. H. Li, *Axisymmetric analytical solutions for a heterogeneous multiferroic circular plate subjected to electric loading*, Mechanics of Advanced Materials and Structures **25**(10) (2018), 795–804.
18. A. J. Dantziger, Multicomponent systems of ferroelectric solid solutions, Physics, Crystallochemistry, Technology. Design Aspects of Piezoelectric Materials, Rostov State Univ. Press, Rostov on Don, V1-2: In Russian, **37**(11) (2001), 1161–1164.
19. E. Mercadelli, A. Sanson, C. Galassi, *Porous piezoelectric ceramics*, IEEE, (2010)

20. A. N. Rybjanets, O. N. Razumovskaya, L. A. Reznitchenko, S. A. Turik, V. A. Alioshin, A. V. Turik, *Porous piezoceramics fabrication methods, mathematical models, experiment*, Izv. Skncvs. Tech. Sci., Spec. Issue **1** (2010), 82–90.
21. J-F. Li, K. Takagi, M. Ono, W. Pan, R. Watanabe, A. Almajid, M. Taya, *Fabrication and evaluation of porous piezoelectric ceramics and porosity–graded piezoelectric actuators*, Journal of the American Ceramic Society **86**(7) (2003), 1094–1098.
22. A. N. Rybjanets, O. N. Razumovskaja, L. A. Reznitchenko, V. D. Komarov, A. V. Turik, *Lead titanate and lead metaniobate porous ferroelectric ceramics*, Integrated Ferroelectrics **63**(1) (2004), 197–200.
23. M. L. Dunn, M. Taya, *Electromechanical properties of porous piezoelectric ceramics*, Journal of the American Ceramic Society **76**(7) (1993), 1697–1706.
24. E. Roncari, C. Galassi, F. Craciun, C. Capiani, A. Piancastelli, *A microstructural study of porous piezoelectric ceramics obtained by different methods* Journal of the European Ceramic Society **21**(3) (2001), 409–417.

ОСНОСИМЕТРИЧНО РЕШЕЊЕ ЗА ЕЛАСТИЧНОСТ НЕДРЕНАЖИРАНОГ ЗАСИЋЕНОГ ПОРО-ПИЕЗОЕЛАСТИЧНОГ ДИСКА

Резиме. У овом раду проучава се кружна плоча израђена од пороеластичне пиезоелектричне керамике. Порозности плоче варирају у зависности од дебљине и осносиметричног понашања пиезоелектричног диска који има хексагоналну материјалну симетрију класе 6 mm. Поред тога, на плочу делују спољна осносиметрична механичка оптерећења у општем облику. Својства материјала плоче експоненцијално варирају као функције променљиве z у цилиндричним координатама. На основу решења за еластичност у односу на радијална и аксијална померања (u, w), добијају се и решавају аналитички парцијалне диференцијалне једначине система. Затим се израчунавају механички напони и електрични помераји. На крају, приказан је пример који илуструје примену изведених формула.

Department of Mechanical Engineering
South Tehran Branch
Islamic Azad University
Tehran
Iran
a_abjadi@azad.ac.ir

Department of Mechanical Engineering
South Tehran Branch
Islamic Azad University
Tehran
Iran
m_jabbari@azad.ac.ir (corresponding author)

Department of Mechanical Engineering
South Tehran Branch
Islamic Azad University
Tehran
Iran
ar_khorshidvand@azad.ac.ir

(Received 11.09.2019.)
(Revised 01.11.2019.)
(Available online 27.12.2019.)